COMMUNICATION

Selective adsorption behaviour of carbon dioxide in OH-functionalized metal–organic framework materials†

Jinjie Qian, [iD] *[ab] Jinni Shen,[b] Qipeng Li, [iD][b] Yue Hu*[a] and Shaoming Huang*[a]

The theoretically optimal adsorption locations in hydroxyl (OH)-decorated metal–organic frameworks show that the captured carbon dioxide (CO_2) molecules interact with the *cis*-μ_2-OH groups in an end-on mode, which shows a moderate to weak hydrogen bond. The experimental isotherms and ideal adsorption solution theory (IAST) calculations show the high selectivity of CO_2 for nitrogen at 273, 283 and 295 K and 1.0 bar for three types of OH-appended isostructures.

The efficient capture and conversion of carbon dioxide (CO_2) is of great importance in realizing a carbon-neutral energy cycle and low-carbon society.[1] Over a long period of time, humans have become heavily reliant on fossil fuels in agriculture and industry, which is widely believed to present the major source for CO_2 emissions, thus leading to the rise of temperatures across the planet, from which a new kind of increasingly serious threat: global warming, may eventually have to be faced.[2] Although several developments of techniques for the capture of CO_2 have been developed, for example, effective and efficient CO_2 adsorption in alkylamine solutions, there are still a series of issues related to cost performance, storage, transportation, and safety with this.[3] Therefore, the strong driving force has long been to use alternative high performance strategies to efficiently remove CO_2.

Currently, microporous metal–organic frameworks (MOFs), a subclass of crystalline hybrid polymers constructed from metallic cations/clusters and organic ligands, are emerging as one of the most promising candidates for CO_2 capture because of their tunable structure, diverse topology, different chemical compositions of the micropores as well as the extra large specific surface area.[4] Within the field of small molecule adsorption, a large amount of research has been focused on the mutual interaction mechanism between the MOF framework and the entrapped small molecule guests, especially for non-polar linear CO_2 molecule, thus discovering new functional materials with better performance. Recently, the group of Ibarra has demonstrated that alcohol confinement within a previously reported water-stable **InOF-1**,[5] built from octahedral indium(III) hydroxide-biphenyltetracarboxylic acid [$In_2(OH)_2(BPTC)$] chain extended by BPTC ligands, can significantly promote CO_2 capture capacity with an approximately 3.6-fold increase of performance (from 3.8 to 13.7 mmol g^{-1}) at only 1.0 bar and 30 °C.[6] In this case, more suitable narrow pore sizes which can effectively accommodate the small guest molecules and thus provide a
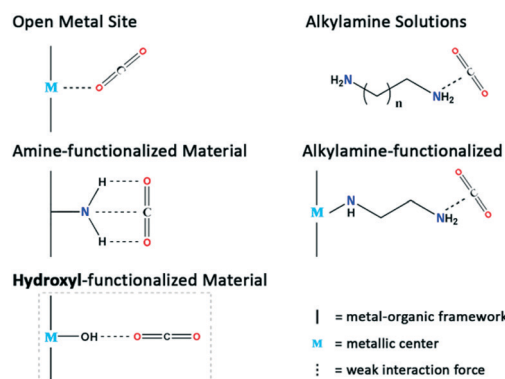

Fig. 1 CO_2 binding interactions in various MOF materials with different functional groups. In an OMS system, the CO_2 molecule uses its central carbon to connect to the MOF metallic center. The alkylamine solution, NH_2-functionalized, and alkylamine-functionalized MOF generally capture CO_2 molecules through a side-on mode, whereas in the OH-functionalized system, the CO_2 molecule attacks the OH group through an end-on mode.

[a] College of Chemistry and Materials Engineering, Wenzhou University, Wenzhou 325035, PR China. E-mail: jinjieqian@wzu.edu.cn, yuehu@wzu.edu.cn, smhuang@wzu.edu.cn; Tel: +86 577 88373064

[b] State Key Laboratory of Structure Chemistry, Fujian Institute of Research on the Structure of Matter, Chinese Academy of Sciences, Fuzhou, Fujian 350002, China

† Electronic supplementary information (ESI) available: For the optimized structures: **Re_GaOF-1** (a = 12.1338, b = 12.1339, c = 12.1338, P1), **Re_GaOF-1** + 4CO₂ (a = 14.9392, b = 14.9392, c = 11.9401, I4122), **Re_InOF-1** (unit cell parameters: a = 12.76990, b = 12.77034, c = 12.76990, P1), **Re_InOF-1** + 4CO₂ (a = 15.7375, b = 15.7375, c = 12.5286, I4122), **Re_AlOF-1** (a = 12.13385, b = 12.13386, c = 12.13385, P1), **Re_AlOF-1** + 4CO₂ (a = 14.9392, b = 14.9392, c = 11.9401, I4122). For more details please see the data in the ESI. See DOI: 10.1039/c7ce01195d

strong overlapping potential have also been confirmed to enhance the CO_2 capacity as well as the sorption affinity.[6] In this respect, it is also necessary to predict and visualize the CO_2 positions in the hydroxyl (OH)-decorated pore environment within the MOF materials using theoretical calculations and experimental tests.

It has been learned that high capacity storage in MOF materials can be achieved by the introduction of open metal sites (OMS),[7a–c] where there exists a strong CO_2 binding strength which forms the $M^{n+}\cdots C(=O)_2$ bond because of the direct interaction between CO_2 and the coordinately unsaturated metal centers, causing irreversible physisorption and permanent loss of OMS activity. Fig. 1 shows that traditional alkylamine solutions, alkylamine-appended as well as polar amine-/sulfonate-/ketone-appended MOF materials[7d–h] can be extensively utilized for the storage and separation of CO_2, but few examples are available showing that OH-functionalized MOF materials can effectively remove CO_2 because of the limited structural stability of the crystal compounds. In this paper, the optimization of CO_2 molecule sites in the **InOF-1** framework using density functional theory (DFT) calculations, and a CO_2 adsorption behaviour comparison with an aluminium-/gallium-(Al/Ga)-based isostructural framework (**AlOF-1** and **GaOF-1**, respectively), is reported, which confirms that all the OH-appended materials possess high CO_2 capacity and selectivity towards nitrogen (N_2) at 273 K, 283 K, and 295 K. Furthermore, it was found that **AlOF-1** outperforms in CO_2 uptake because of the large binding energy used to structurally form **AlOF-1·4CO₂**. More importantly, a high selectivity of CO_2/N_2 at 273–295 K and 1.0 bar, and a large heat of CO_2 adsorption can be achieved at zero coverage (20.37 kJ mol⁻¹ for **AlOF-1**, 18.31 kJ mol⁻¹ for **GaOF-1** and 11.98 kJ mol⁻¹ for **InOF-1**).

The pristine **InOF-1** and ethanol (EtOH)-impregnated **InOF-1** (**InOF-1–EtOH**) simultaneously exhibit an outstanding CO_2 capacity under the same conditions.[6] Therefore, it is of great importance to understand the in-depth mechanism for the binding formation of small molecules and their hosts using direct visualization of the interaction between the CO_2 molecules and the **InOF-1** framework. In this paper, the adsorption of CO_2 in one water-stable tetracarboxylate-based framework with an In(III) metal cation, [**InOF-1**, Fig. 2a and b and S2 (ESI†)] is mainly predicted and explained using DFT calculations. Meanwhile, the electron and energy properties of **InOF-1** were calculated using a combination of DFT and plane-wave pseudopotential methods as implemented in the Vienna *Ab initio* Simulation Package (VASP) code.[8] Calculations were performed under the Perdew–Burke–Ernzerhof (PBE) approximation[9] for exchange and correlation with a plane-wave cutoff energy of 380 eV. The optimized unit cell
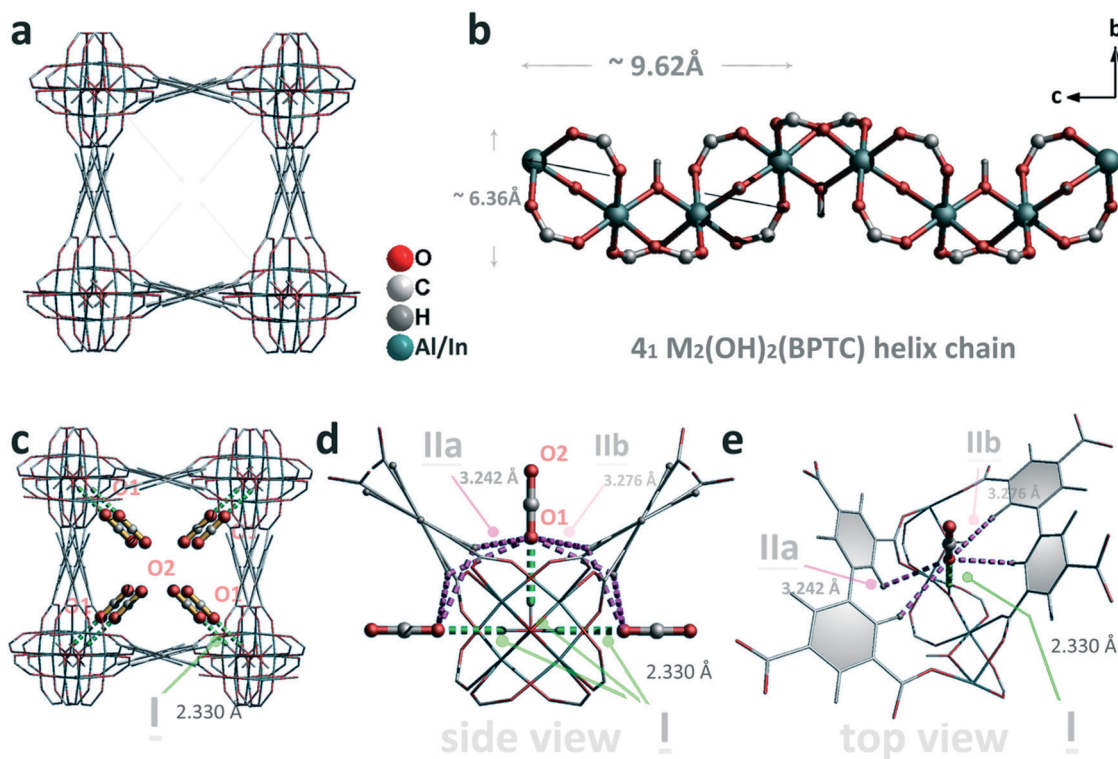

Fig. 2 Theoretically optimized CO_2 positions in the tetragonal channels of two isostructural M-BPTC frameworks. (a) View of the 3-dimensional structure with a square channel. The *cis*-μ_2-OH groups protrude into the center of the channel from four directions. (b) View of the corner sharing octahedral [$M_2(OH)_2(BPTC)$] chain along the *a* axis. The different sizes of the 4_1 chain are highlighted. (c) View of the structure of M-BPTC·4CO₂ obtained using a combination of DFT and plane-wave pseudopotential methods as implemented in the VASP software. The adsorbed CO_2 molecules in the channel are highlighted by the use of the ball-and-stick mode. The interactions between CO_2 molecules and μ_2-OH groups are highlighted in green. (d and e) Detailed views of the roles of the –OH and –CH groups in binding CO_2 molecules in a pocket-like cavity.

used has 72 and 84 atoms for the bare and four CO_2 molecules loaded materials (**InOF-1·4CO₂**, where each μ_2-OH group only connects to one CO_2 molecule), respectively. The wave functions were sampled according to the Monkhorst–Pack scheme with a k-point with mesh spacing of ~0.05 Å^{-1}.

As well as the **InOF-1** material, two other isostructural host **AlOF-1** and **GaOF-1** were also prepared,[7d–f] and these possess a hydroxyl-functionalized 4_1 $M_2(OH_2)(BPTC)$ helix chain (M = Al or Ga), whose sizes are ~6.36 × 9.62 Å^2 (Fig. 2b). DFT calculations were used to refine the crystal structure for the optimized **InOF-1·4CO₂** structures, and this shows that these adsorbed CO_2 molecules interact with the cis-μ_2-OH groups in an end-on mode (Fig. 2c). The O···H distance (d_I) between the entrapped CO_2 molecule and the hydroxyl group (H_{OH}) is 2.330 Å which indicates a relatively moderate to weak hydrogen bond (Table 1). The optimized C–O bond lengths in CO_2 were 1.179 Å (hydrogen bonded end, C–O1) and 1.173 Å (free end, C–O2), and the ∠OCO bond angle was absolutely linear and had a value of 180°. For the coordination environment of each captured CO_2 molecule, the hydrogen bonded O1 atom was also bolstered together by weak cooperative supramolecular interactions between the O1 atom and H atoms from biphenyl C–H groups (H_{CH}, O···H = 3.242 Å and 3.276 Å for d_{IIa} and d_{IIb}, respectively, and each occurs twice, Fig. 2d). In this context, the d_{IIa} and d_{IIb} distances in the **InOF-1·4CO₂** and **GaOF-1·4CO₂** structure (d_{IIb} = 3.202 Å) are slightly larger than that of the **AlOF-1·4CO₂** structure (d_{IIa} = 3.124 Å, d_{IIb} = 3.197 Å, see Table 1), which obviously indicates more strong interactions between the main MOF framework and the captured CO_2 molecules in the **AlOF-1** parent. A top view of the adsorbed CO_2 molecule in the OH-functionalized in-based chain, a total of 5 H atoms (4 H_{CH} atoms and 1 H_{OH} atom) attract cooperatively with the O1 charge centres of the captured CO_2 molecules in the tetragonal channel through the combination of the moderate to weak hydrogen bonds and the supramolecular interactions (Fig. 2e). As shown in Fig. 2c–e, the modest hydrogen bond between the O1 atom and the H_{OH} atom from the M–OH moiety is highlighted in green, and the weak cooperative hydrogen-bond interactions between O1 and H_{CH} H(dp) from the C–H groups are highlighted in pink for clarity and comparison.

However, in order to reveal the theory of the adsorption of CO_2 in these three types of isostructures, the binding energy (ΔE), zero point energy correction (ZPEC), thermal energy correction (TEC) and binding enthalpy (ΔH) of **AlOF-1·4CO₂**, **GaOF-1·4CO₂** and **InOF-1·4CO₂** were calculated.

The ΔE of CO_2 is evaluated using the following equation:

$$\Delta E = -E_{MOF·4CO_2} + E_{MOF} + 4E_{CO_2} \qquad (1)$$

in which $E_{MOF·4CO_2}$ is the total energy of the framework and the adsorbed CO_2 molecule, E_{MOF} and E_{CO_2} are the energies of the framework and the CO_2 molecule, respectively.

The ZPEC for a system is then calculated as:[10]

$$ZPEC = ZPE_{MOF·4CO_2} - ZPE_{MOF} - 4ZPEB_{CO_2} \qquad (2)$$

where MOF and CO_2 are systems that are considered in isolation and then in combination as MOF·4CO₂ to determine the change in ZPE that results from the systems being placed in the presence of one another.

Similar to ZPEC, TEC is also t calculated as follows:[10]

$$TEC = TE_{MOF·4CO_2}(T) - TE_{MOF}(T) - 4TE_{CO_2}(T) \qquad (3)$$

where MOF, CO_2 and MOF + CO_2 are as stated previously.

The binding enthalpies at a given temperature are calculated as:[10]

$$-\Delta H(T) = H(T)_{MOF·4CO_2} - H(T)_{MOF} - 4H(T)_{CO_2} \qquad (4)$$

where $H(T)_{MOF}$, $H(T)_{CO_2}$, and $H(T)_{MOF·4CO_2}$ are the enthalpy of the bare MOF without the guest molecule, the enthalpy of the molecule in the gas phase, and the enthalpy of the MOF with the molecule adsorbed, respectively, all at temperature, T. A positive $\Delta H(T)$ corresponds to an exothermic adsorption.

The previously described calculated energies are summarized in Table 1. In this table, the larger ΔE and ΔH represent stronger binding. Larger ZPEC and TEC values represent greater correction, that is to say, **AlOF-1** (ZPEC = 9.910 kJ mol^{-1}, TEC = 35.827 kJ mol^{-1}) tends to possess greater correction with CO_2 than both **GaOF-1** and **InOF-1**. A stronger binding generates greater confinement and a steeper potential well, and thus yields a larger ZPEC but less thermal motion inside the well.[10] This means that **AlOF-1·4CO₂** is easier to form than **GaOF-1·4CO₂** or **InOF-1·4CO₂**. Consequently, agreement is achieved between the previously reported results and this data.

To compare the previously calculated results with experimental CO_2 adsorption tests, **InOF-1**, **AlOF-1** as well as **GaOF-1** materials were synthesized according to previous methods reported in the literature for better comparison.[5a,7d,f,11] In order to confirm the permanent porosity, the N_2 isotherms at 77 K were first determined prior to the CO_2 sorption test. The desolvated **InOF-1** and **GaOF-1** samples showed totally reversible type-I isotherms with the maximum uptake value of 270.9/131.1 m^3 g^{-1} at 1.0 bar and 77 K which corresponds to a Brunauer–Emmett–Teller (BET) and Langmuir surface area of 1065/1093 m^2 g^{-1} and 517/570 m^2 g^{-1}, respectively. In contrast, the activated **AlOF-1** powder exhibited barely any N_2 sorption

Table 1 The specific bond is listed (in Å units) and the binding energy, zero point energy, thermal energy and binding enthalpy at 300 K (in kJ mol^{-1})

Items	AlOF-1·4CO₂	GaOF-1·4CO₂	InOF-1·4CO₂
d_{C-O1} (Å)	1.178	1.176	1.179
d_{C-O2} (Å)	1.174	1.170	1.173
d_I (Å)	2.487	2.289	2.330
d_{IIa} (Å)	3.124	3.086	3.242
d_{IIb} (Å)	3.197	3.202	3.276
ΔE (kJ mol^{-1})	17.078	15.970	15.953
ZPEC (kJ mol^{-1})	9.190	8.069	6.068
TEC (kJ mol^{-1})	35.827	32.663	27.077
ΔH (kJ mol^{-1})	78.341	65.568	60.215

capacity at 77 K, with a maximum value of only 13.4 cm^3 g^{-1} at 1.0 bar and 77 K (Fig. 3a). Despite the microporous window size and the rigid framework for **AlOF-1**, it was surprising that the low N_2 diffusion into the voids can be observed at 77 K. It was assumed this behaviour might be derived from a strong interaction between the nitrogen molecules and the narrow pore windows by the considerable quadrupole interactions with the electrostatic field gradients near the surface, which subsequently prohibit other molecules from penetrating into the voids,[12] because the **AlOF-1** framework possesses only open 1-dimensional channels along the c-axis.

Most importantly, the fascinating internal OH-suspended tetragonal tubes inevitably prompt the further investigation of the practical CO_2 sorption capacity. Single component low-pressure gas sorption isotherms for the three types of desolvated samples toward CO_2 at 273 K, 283 K, and 295 K were collected using a volumetric measurement method and the results obtained are presented in Fig. 4a and Fig. S9–11 (ESI†). Compared to its very low sorption for N_2, the CO_2 isotherms of **AlOF-1** at the specific temperatures (273–295 K) show extremely high sorption capacities, with the saturated value of 155.5 cm^3 g^{-1} (6.94 mmol g^{-1}, 305.4 mg g^{-1}) at 273 K and 1.0 bar. Meanwhile, it was also found that the CO_2 adsorption curve quickly reached the value of 42.6 cm^3 g^{-1} (1.90 mmol g^{-1}, 83.7 mg g^{-1}) at 0.15 bar, which is lower than the equivalent partial pressure in flue gas (Fig. 4a). Obviously, this capacity surpasses the **InOF-1** adsorption value of 39.1 cm^3 g^{-1} (1.75 mmol g^{-1}, 76.8 mg g^{-1}) at 273 K and 0.15 bar and 140.1 cm^3 g^{-1} (6.25 mmol g^{-1}, 275.2 mg g^{-1}) at 273 K and 1.0 bar. Similar trends can also be found in the uptake of CO_2 at 1.0 bar and 283 K and 295 K, where the **AlOF-1** shows a good performance with 118.6 cm^3 g^{-1} and 86.7 cm^3 g^{-1}, respectively, whereas the **InOF-1** exhibits a lower capability towards CO_2 with 109.5 cm^3 g^{-1} at 283 K and 83.9 cm^3 g^{-1} at 295 K. Furthermore, in terms of CO_2 storage, the Ga-based material shows the lowest capability of 90.3, 71.6 and 56.6 cm^3 g^{-1} [Fig. 4b and S15 (ESI†)]. In this case, it was speculated that there exists a strong interaction between the solvent molecules and the **GaOF-1**
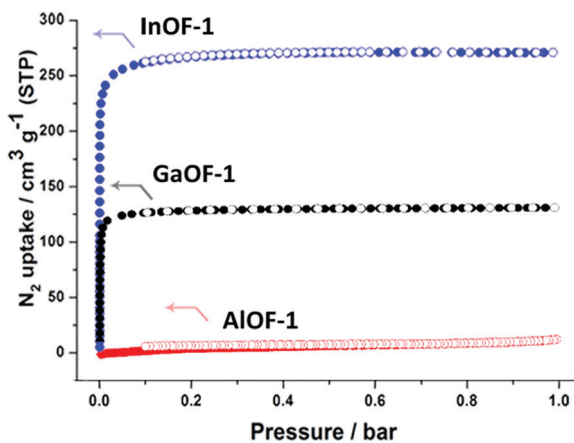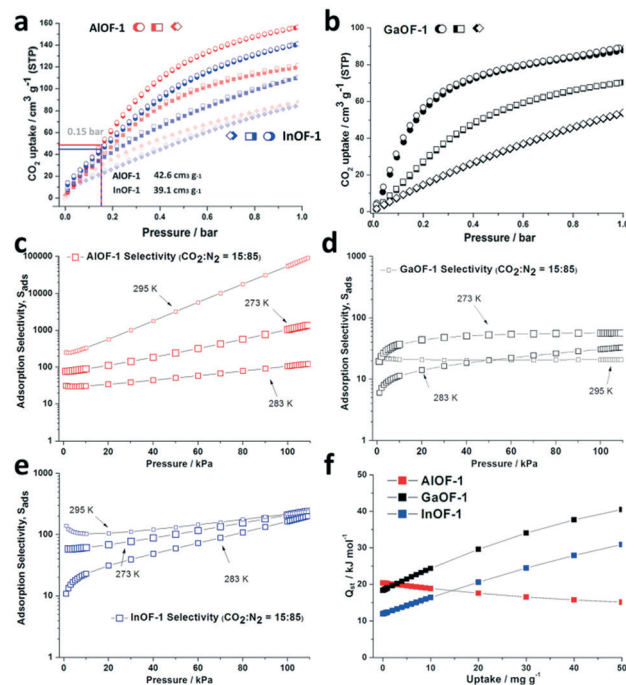

Fig. 4 (a) and (b) Experimental CO_2 sorption isotherms at 273 K (● adsorption, ○ desorption), 283 K (■ adsorption, □ desorption) and 295 K (♦ adsorption, ◇ desorption). (c)–(e) The selectivity between CO_2 and N_2 at three different temperatures for **AlOF-1**, **GaOF-1** and **InOF-1**. (f) The adsorption heat (Q_{st}) of CO_2 for the three types of isostructural M–BPTC materials fitted using the virial method.

framework, thus leading to the incomplete desolvation and inadequate utilization of the expected pore volume. However, it should be noted that the CO_2 capacity of **AlOF-1** and **InOF-1** materials gradually gets closer when the temperature is elevated from 273 K to 295 K (Fig. 4a), which means that the active CO_2 spacing in **AlOF-1** is lost faster than that in **InOF-1**. However, a large amount of CO_2 is still retained under these different temperatures, especially for the Al-based framework, which indicates the excellent retention of the microporous nature before and after the desolvation treatment and gas sorption, as shown in Fig. S6 and S7 (ESI†).

Finally, the IAST prediction based upon the experimental CO_2 and N_2 isotherms are clearly presented in Fig. 4b. The adsorption selectivity is defined as $S_{i/j} = (q_1/q_2)/(p_1/p_2)$, in which q_i is the amount of i adsorbed and p_i is the partial pressure of i in the mixture. At 1.0 bar, the calculated CO_2/N_2 selectivities for **AlOF-1** are more variable: 1078.8 and 108.4 at 273 K and 283 K from gas–phase mixtures in a 15 : 85 molar ratio, whereas at 295 K, it reaches an excessive amount of 58 571.6 because of the very low capacity of N_2 at 1.0 bar. Compared to that of the Al-based material, the theoretically calculated CO_2/N_2 selectivity values for **GaOF-1** and **InOF-1** are more reasonable and trustworthy, where they are 56.7/212.6, 31.1/168.1 and 20.8/219.6 at 273, 283 and 295 K, respectively, [Fig. 4c–e, S20–22 (ESI†)]. More interestingly, the heat of CO_2 adsorption at zero coverage is calculated to be 20.37 kJ mol^{-1} (**AlOF-1**), 18.31 kJ mol^{-1} (**GaOF-1**), and 11.98 kJ mol^{-1} (**InOF-1**) based on the CO_2

Fig. 3 N_2 adsorption/desorption isotherms at 77 K for **AlOF-1**, **GaOF-1** and **InOF-1**. ● adsorption, ○ desorption.

isotherms at 283 K and 295 K, which indicates a more reasonable order for this series of M-BPTC structures despite the deficient performance for **GaOF-1** in the CO_2 sorption analysis (Fig. 4f). These calculations and observation indicate that all the OH-functionalized materials are promising candidates for practical CO_2 capture and conversion applications.

In summary, with a combination of theoretical calculations and experimental tests, the role of group A(III) metals in three types of OH-appended M-BPTC MOFs, including **AlOF-1**, **GaOF-1** and **InOF-1** were thoroughly compared. In this series, it was found that the CO_2 binding to the *cis*-μ_2-OH groups is in an end-on mode and this is further supported by H-bonding with adjacent biphenyl rings. The experiments and IAST results demonstrate that the largest binding energy and adsorption heat exist in the Al(III)–OH···C(=O)$_2$ system which could be empirically predicted by the atomic mass of the cations in the isostructural frameworks. This research provides a useful guideline for the future development of versatile MOFs with functionalized groups.

Conflicts of interest

There are no conflicts to declare.

Acknowledgements

Notes and references

1 (a) A. Schoedel, Z. Ji and O. M. Yaghi, *Nat. Energy*, 2016, **1**, 16034; (b) N. Kornienko, Y. B. Zhao, C. S. Kley, C. H. Zhu, D. Kim, S. Lin, C. J. Chang, O. M. Yaghi and P. D. Yang, *J. Am. Chem. Soc.*, 2015, **137**, 14129–14135.

2 C. McGlade and P. Ekins, *Nature*, 2015, **517**, 187–190.

3 (a) G. T. Rochelle, *Science*, 2009, **325**, 1652–1654; (b) R. Idem, M. Wilson, P. Tontiwachwithikul, A. Chakma, A. Veawab, A. Aroonwilas and D. Gelowitz, *Ind. Eng. Chem. Res.*, 2006, **45**, 3414; (c) N. Planas, A. L. Dzubak, R. Poloni, L. C. Lin, A. McManus, T. M. McDonald, J. B. Neaton, J. R. Long, B. Smit and L. Gagliardi, *J. Am. Chem. Soc.*, 2013, **135**, 7402–7405.

4 (a) Y. Yan, M. Juríček, F. Coudert, N. A. Vermeulen, S. Grunder, A. Dailly, W. Lewis, A. J. Blake, J. F. Stoddart and M. Schröder, *J. Am. Chem. Soc.*, 2016, **138**, 3371–3381; (b) J. M. Lin, C. T. He, Y. Liu, P. Q. Liao, D. D. Zhou, J. P. Zhang and X. M. Chen, *Angew. Chem., Int. Ed.*, 2016, **55**, 4674–4678; (c) J. R. Ramirez, H. Y. Yang, C. M. Kane, A. N. Ley and K. T. Holman, *J. Am. Chem. Soc.*, 2016, **138**, 12017–12020; (d) A. J. Rieth, Y. Tulchinsky and M. Dincă, *J. Am. Chem. Soc.*, 2016, **138**, 9401–9404; (e) L. F. Liang, Q. H. Chen, F. L. Jiang, D. Q. Yuan, J. J. Qian, G. X. Lv, H. Xue, L. Y. Liu, H. L. Jiang and M. C. Hong, *J. Mater. Chem. A*, 2016, **4**, 15370–15374;

(f) G. Y. Zhang, G. F. Wei, Z. P. Liu, S. R. J. Oliver and H. H. Fei, *Chem. Mater.*, 2016, **28**, 6276–6281; (g) G. F. Feng, Y. X. Peng, W. Liu, F. F. Chang, Y. F. Dai and W. Huang, *Inorg. Chem.*, 2017, **56**, 2363–2366.

5 (a) J. J. Qian, F. L. Jiang, D. Q. Yuan, M. Y. Wu, S. Q. Zhang, L. J. Zhang and M. C. Hong, *Chem. Commun.*, 2012, **48**, 9696–9698; (b) M. Savage, Y. Q. Cheng, T. L. Easun, J. E. Eyley, S. P. Argent, M. R. Warren, W. Lewis, C. Murray, C. C. Tang, M. D. Frogley, G. Cinque, J. L. Sun, S. Rudić, R. T. Murden, M. J. Benham, A. N. Fitch, A. J. Blake, A. J. Ramirez-Cuesta, S. H. Yang and M. N. Schröder, *Adv. Mater.*, 2014, **28**, 8705–8711; (c) M. Savage, I. da Silva, M. Johnson, J. H. Carter, R. Newby, M. Suyetin, E. Besley, P. Manuel, S. Rudić, A. N. Fitch, C. Murray, W. I. F. David, S. H. Yang and M. Schröder, *J. Am. Chem. Soc.*, 2016, **138**, 9119–9127.

6 R. A. Peralta, A. Campos-Reales-Pineda, H. Pfeiffer, J. R. Álvarez, J. A. Zárate, J. Balmaseda, E. González-Zamor, A. Martínez, D. Martínez-Otero, V. Jancik and I. A. Ibarra, *Chem. Commun.*, 2016, **52**, 10273–10276.

7 (a) W. Zhou, H. Wu and T. Yildirim, *J. Am. Chem. Soc.*, 2008, **130**, 15268–15269; (b) E. D. Bloch, W. L. Queen, R. Krishna, J. M. Zadrozny, C. M. Brown and J. R. Long, *Science*, 2012, **335**, 1606–1610; (c) T. M. McDonald, J. A. Mason, X. Kong, E. D. Bloch, D. Gygi, A. Dani, V. Crocella, F. Giordanino, S. O. Odoh, W. Drisdell, B. Vlaisavljevich, A. L. Dzubak, R. Poloni, S. K. Schnell, N. Planas, K. Lee, T. Pascal, L. F. Wan, D. Prendergast, J. B. Neaton, B. Smit, J. B. Kortright, L. Gagliardi, S. Bordiga, J. A. Reimer and J. R. Long, *Nature*, 2015, **519**, 303–308; (d) S. H. Yang, J. L. Sun, A. J. Ramirez-Cuesta, S. K. Callear, W. I. F. David, D. P. Anderson, R. Newby, A. J. Blake, J. E. Parker, C. C. Tang and M. Schröder, *Nat. Chem.*, 2012, **4**, 887–894; (e) S. H. Yang, A. J. Ramirez-Cuesta, R. Newby, V. Garcia-Sakai, P. Manuel, S. K. Callear, S. I. Campbell, C. C. Tang and M. Schröder, *Nat. Chem.*, 2015, **7**, 121–129; (f) C. P. Krap, R. Newby, A. Dhakshinamoorthy, H. García, I. Cebula, T. L. Easun, M. Savage, J. E. Eyley, S. Gao, A. J. Blake, W. Lewis, P. H. Beton, M. R. Warren, D. R. Allan, M. D. Frogley, C. C. Tang, G. Cinque, S. H. Yang and M. Schröder, *Inorg. Chem.*, 2016, **55**, 1076–1088; (g) R. Vaidhyanathan, S. S. Iremonger, G. K. H. Shimizu, P. G. Boyd, S. Alavi and T. K. Woo, *Science*, 2010, **330**, 650–653; (h) T. Panda, P. Pachfule, Y. F. Chen, J. W. Jiang and R. L. Banerjee, *Chem. Commun.*, 2011, **47**, 2011–2013.

8 G. Kresse and D. Joubert, *Phys. Rev. B: Condens. Matter Mater. Phys.*, 1999, **59**, 1758–1775.

9 J. P. Perdew, K. Burke and M. Ernzerhof, *Phys. Rev. Lett.*, 1996, **77**, 3865–3868.

10 (a) K. Lee, J. D. Howe, L. C. Lin, B. Smit and J. B. Neaton, *Chem. Mater.*, 2015, **27**, 668–678; (b) K. Tan, S. Zuluaga, Q. H. Gong, Y. Z. Gao, N. Nijem, J. Li, T. Thonhauser and Y. J. Chabal, *Chem. Mater.*, 2015, **27**, 2203–2217.

11 T. Panda, S. Horike, K. Hagi, N. Ogiwara, K. Kadota, T. Itakura, M. Tsujimoto and S. Kitagawa, *Angew. Chem.*, 2017, **129**, 2453–2457.

12 (a) K. M. Ok, J. Sung, G. Hu, R. M. J. Jacobs and D. O'Hare, *J. Am. Chem. Soc.*, 2008, **130**, 3762–3763; (b) T. K. Maji, R. Matsuda and S. Kitagawa, *Nat. Mater.*, 2007, **6**, 142–148.